Observing During Bright Time: Tips and Tricks

In this paper we present and discuss the effects of scattered moonlight on optical observations, the current status of the moonlit night sky modelling and the implications this has on the Service Mode observations and the maximisation of scientific outcome.

Ferdinando Patat

User Support Dept. - ESO, DMD

EVEN THOUGH it is certainly one of the most fascinating celestial objects, the moon is indeed a disturbing companion when one is to push ground-based telescopes and instruments to their limits, since it causes a significant increase in the sky brightness, at least in the UV and optical domains (see Fig. 1 for a real example). This is why such observations are usually carried out during dark time, when the sky brightness reaches its minimum values. In general, the effect of an enhanced night sky emission translates into an increased background photon shot noise, which in turn, degrades the signal-to-noise one can reach in the science exposures. For example, in the most extreme case of full moon, the night sky in the *B*-band is typically four magnitudes brighter than during dark time. For any given exposure time, this causes the signal-to-noise ratio of background dominated images to decrease by more than a factor of six with respect to the same exposure obtained in dark time. Of course, not all astronomical observations need dark conditions and, depending on the apparent luminosity of the targets, they can be successfully carried out with a moderate contribution by the moon. In some extreme cases, like high-resolution spectroscopy of bright stars, the observations can be safely performed even with full moon.

In an era when Service Mode appears to be the most efficient way of operating large telescopes, it is clear that having a tool for setting the moon constraints in an optimal way would increase the chances that a given programme is effectively executed. For these reasons, the quantitative study of the moon impact on astronomical observations is an important task, which most large ground-based observatories are starting to pursue.

In this paper we will present the effects of moonlight, the basic ingredients that contribute to the physical problem, the current status of modelling and we will finally discuss the future perspectives.

Figure 1: Image taken by the ESO Mini All-Sky Cloud Observation Tool (MASCOT) on 19-09-2004, when the moon was at 16 degrees above the horizon and the fractional lunar illumination (FLI) was 0.2. The greyscale is logarithmic and the bright circular structure visible in the upper right corner of the image is a reflection within the camera optics.

A Spectrum of the Moonlit Night Sky

An example of the moon effects on the night sky is shown in Fig. 2, where we have plotted a low-resolution spectrum taken with FORS1 on the first of September 2004. On that night, the moon was almost full and, at the time of the observation, it was shining at an elevation of about 55 degrees above the horizon and at an angular distance of 30 degrees from the direction pointed by UT2-Kueyen, at an elevation of 65 degrees. For comparison we have also plotted a night sky spectrum obtained at Paranal in dark time (see Patat 2003). Several interesting aspects emerge from this comparison. First of all, the moonlit sky spectrum is dominated by a rather blue continuum, which peaks at about 450 nm, right at the centre of the *B* passband. In the specific example shown in Fig. 2, the night sky is about 25 times (i.e. 3.5 magnitudes) brighter than in dark time in this wavelength range. For *V, R* and *I* this difference reduces to 2.9, 2.4 and 1.3 magnitudes respectively. The synthetic (*B–V*) colour of the moonlit night sky turns out to be about 0.4, while (*B–V*)=1.0 is the typical

value one measures during dark time (see for example Patat 2003).

Another interesting feature is the appearance of absorption lines, especially in the bluer part of the spectrum. One can in fact easily identify the hydrogen Balmer lines (H_α, H_β, H_γ and so on), the so-called *G*- band (430 nm), Mg I (517, 518 nm) and the prominent H&K CaII lines (393, 397 nm) at the red edge of the Balmer jump. Of course, all these spectral features and the stellar continuum are an imprint of the solar spectrum, which is reflected by the moon and scattered into the line of sight by Earth's atmosphere. To illustrate this effect, in Fig. 2 we have overplotted the model spectrum for the sun (Kurucz, 1993). What one can immediately notice is that the moonlit night sky spectrum is definitely bluer than the solar spectrum, for which it is in fact (*B–V*)=0.65, and the difference is particularly marked at wavelengths shorter than 400 nm. Finally, as one goes into the red, the contribution by the solar continuum becomes less and less relevant and, at wavelengths longer than 900 nm, the emission bands produced by the atmospheric OH are
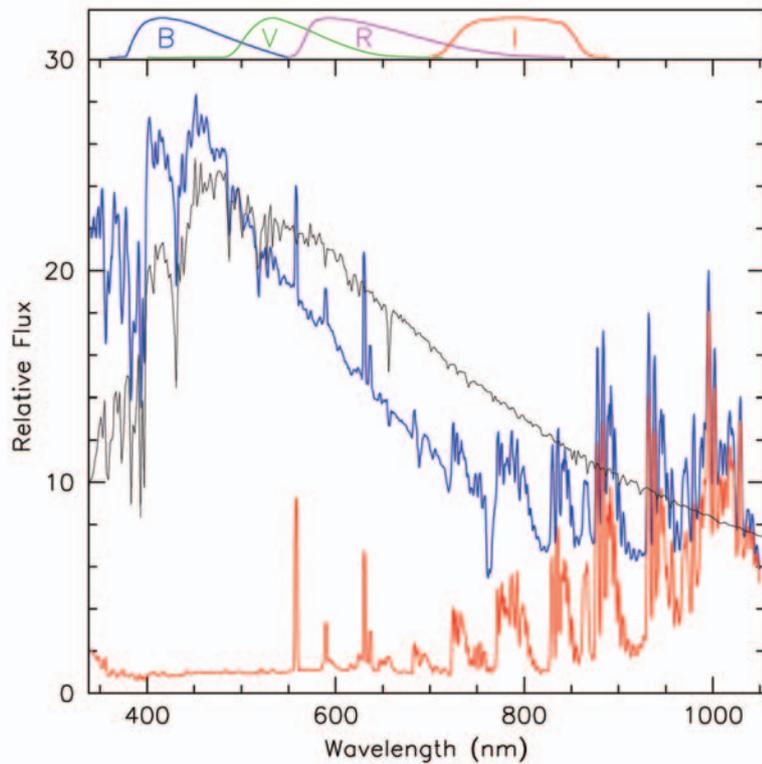
Figure 2: Comparison between the night sky spectrum during dark time (red line, Patat 2003) and bright time (blue line). The latter was obtained with FORS1 on September 1, 2004 using the low dispersion grism 150I and no order sorter filter. Due to the very blue continuum, the spectral region at wavelengths redder than 650 nm is probably contaminated by the grism second order. Both spectra have been normalized to the continuum of the first one at 500 nm. For comparison, the model spectrum of a solar-type star is also plotted (black line). For presentation, this has been normalized to the moonlit night sky spectrum at 500 nm. The upper plot shows the standard *BVRI* Johnson-Cousins passbands.
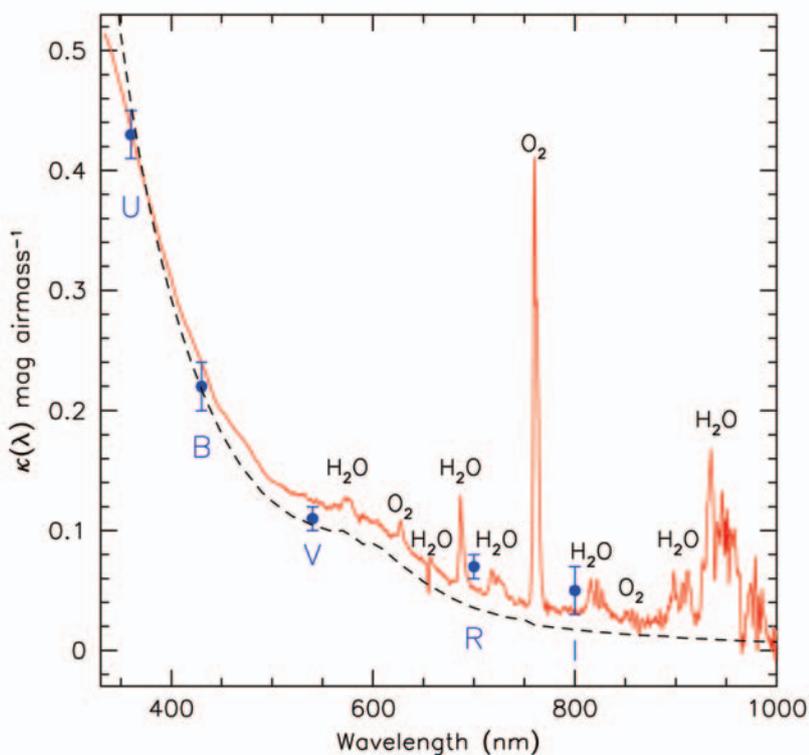
Figure 3: Atmospheric extinction at Paranal estimated from FORS1 observations of the spectrophotometric standard star EG274 (red line). For comparison, the *UBVRI* broadband measurements (filled circles, Patat 2003) and a standard atmosphere model including Air molecules, Ozone and Aerosols (dashed line, Hayes & Latham 1975) are also plotted.

the prominent source of night sky radiation. At even longer wavelengths, in the near-IR, they then completely dominate the night sky emission, even in the presence of full moon. The wavelength dependence on the moonlit night sky spectrum is in fact dictated by two different ingredients: the input source spectrum, that we have just seen, and the physical characteristics of the Earth's atmosphere, which is the topic of the next section.

ATMOSPHERIC EXTINCTION

The physical processes that take place in the scattering of moonlight are exactly the same that are at work during daytime, when the sun illuminates the atmosphere. The amount of radiation reflected at a given wavelength and in a given direction depends on the physical properties of the scattering elements. In the case of Earth's atmosphere, these are mainly identified as molecules of air, water and Ozone (O_3) and, to a smaller extent, the so-called aerosols, which include dust, salt particles and water droplets. These are of course responsible also for the atmospheric extinction, which is just another manifestation of the same phenomenon. In fact, on the one hand the scattering brings the incoming photons out of the line of sight, while on the other it averts photons originally arriving out of the line of sight into the observer's direction.

Therefore, in order to understand the diffusion of moonlight at a given astronomical site, one first needs to study the atmospheric extinction as a function of wavelength. This can be easily done taking spectra of bright stars at different airmasses. An example for the case of Paranal is shown in Fig. 3, where we have plotted the extinction coefficient $\kappa(\lambda)$ computed from FORS1 archival data. At wavelengths bluer than 500 nm the extinction shows a very steep increase, which is due to the well-known λ^{-4} Rayleigh scattering by the Air molecules and which is the responsible for the blue colour of the daytime sky. At longer wavelengths (500-650 nm), the extinction is dominated by the scattering produced by aerosols, which shows a much flatter behaviour (λ^{-a}, with a=0.5–0.9). Finally, water vapour is the dominant source of absorption for $\lambda > 700$ nm, accompanied also by some O_2 bands between 650 and 1000 nm. These features strongly change with time and site and for this reason are pretty difficult to model (see for example Hayes & Latham 1975). Given the wavelength dependency of the $\kappa(\lambda)$ function, and as in the case of the daylight, the moonlit night sky is bluer than the input light source. Therefore, the effect of moonlight is stronger in the blue, both because of the input source spectrum and the higher scattering efficiency. Below 475 nm, the increase in the extinction coefficient is compensated by the decrease of the solar flux (see Fig. 2) and this causes the observed spectrum to remain rather flat. Finally, due to the increased thickness of the atmosphere, the amount of scattered light is expected to be in general higher at higher airmasses, causing the sky to become brighter towards the horizon. This
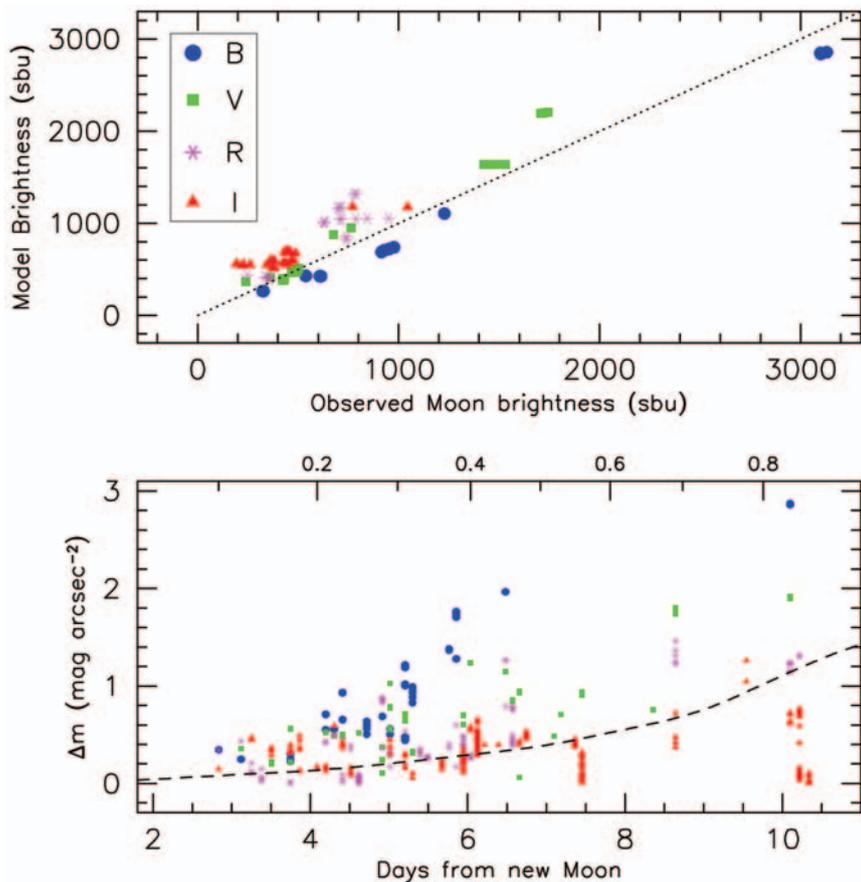
Figure 4: Lower panel: observed sky brightness as a function of moon age for *B, V, R* and *I* (Patat 2003). The solid curve traces the data published by Walker (1987) for the *V* passband, while the upper scale shows the fractional lunar illumination. Upper panel: comparison between observed and predicted moon contribution (Krisciunas & Schaefer 1991). Surface brightness is expressed in surface brightness units (1 sbu = 10^{-8} W m^{-2} μm^{-1} sr^{-1}).

is in fact clearly visible in the image presented in Fig. 1.

MOONLIGHT MODELLING

Of course, when one is to predict the sky brightness enhancement produced by the presence of the moon at a given position in the sky, besides the atmospheric extinction, several other parameters have to be taken into account. First of all, one would have to know the moon's albedo as a function of wavelength, in order to correctly compute the input spectrum at the top of the atmosphere. Then, since the scattering efficiency is generally a function of wavelength and scattering angle, one would have to characterize these functions for the different molecules and particulates present in the atmosphere. For example, Air molecules produce a Rayleigh scattering, while aerosols (which are responsible of phenomena like the aureole) rather produce a Mie scattering (see for example the classical textbook by v. d. Hulst 1957).

An approximate approach, which to our knowledge is the only one available in the literature, is that proposed by Krisciunas & Schaefer (1991, hereafter KS) for the *V* passband and its generalization to the whole UBVRI photometric system (Schaefer 1998). In the KS treatment, the expected sky brightness depends in the extinction coefficient κ(λ), the apparent magnitude of the moon (which is usually parameterised with the Fractional Lunar Illumination, or FLI), its zenith distance, the angular separation between the moon and the target and the zenith distance of the target itself. Another fundamental ingredient is the function that describes the dependence of scattering efficiency from the scattering angle, which practically coincides with the moon-target angular separation. The KS model includes both Rayleigh and Mie scattering expressions for this function and it has been calibrated using daytime sky brightness measurements. It is important to notice that this function shows a minimum at 90 degrees, which is therefore the angular distance at which the contribution is expected to reach its minimum. As we will see below, this distance is actually decreased by the effects of airmass. The model accuracy in the *V* passband was tested by the authors, who reported root mean square deviations as large as 23% in a brightness range that spans over 20 times the typical value observed during dark time. These can be attributed to the model approximations but also to fluctuations in the atmospheric conditions (aerosols, thin cirrus clouds).

Even though FORS1 is typically a dark time instrument, some data are obtained when the moon contribution to the sky brightness is conspicuous and this gave us the possibility of directly measuring its effect and comparing it with the KS model in the other passbands (see Patat 2003). To estimate the fraction of sky brightness generated by scattered moonlight, one simply needs to subtract the dark time estimates to the observed fluxes for each passband. The results of this operation are presented in the lower panel of Fig. 4. As expected, the largest deviations are seen in *B*, where the sky brightness can increase by about 3 magnitudes at 10 days after new moon, while in I, at roughly the same moon age, this deviation just reaches about 1.2 magnitudes. It is interesting to note that most exposure time calculators for modern instruments make use of the function published by Walker (1987) to compute the expected sky brightness as a function of moon age. As already noticed by Krisciunas (1990), this gives rather optimistic estimates, real data being most of the time noticeably brighter. This is clearly visible in Fig. 4, where we have overplotted Walker's function for the *V* passband on our data: already at six days past new moon the observed *V* data (green squares) show maximum deviations of the order of one magnitude. These results are fully compatible with those presented by Krisciunas (1990). Clearly, a one-parameter description (i.e. moon phase) is not enough to predict with sufficient accuracy the sky brightness. In this respect, the KS model is much more promising, since it takes into account all relevant astronomical circumstances, some of which, admittedly, are known only when the time the target is going to be observed is known. This limits the applicability to a "nowcast" by the observer rather than a forecast by the user, an important issue which we will come back to at the end of the paper.

In the upper panel of Fig. 4 we have compared our results with the KS model predictions, including *B, V, R* and *I* data. We emphasise that we have used average values for the extinction coefficients and dark time sky brightness of Paranal and this certainly has some impact on the computed values. The unaccounted presence of thin cirrus clouds can also cause significant deviations. On the other hand, this is the typical configuration under which the procedure would be implemented in an exposure time calculator, and hence it gives a realistic evaluation of the model practical accuracy. Figure 4 shows that, even if maximum deviations as large as 0.4 magnitude are present, the model gives a reasonable reproduction of the data in the brightness range covered by our observations. This is actually less than half the one encompassed by the *V*-band data used by KS, which reach about 8300 sbu. For comparison, the typical dark time sky brightness in *V* is about 370 sbu (Patat 2003). Another feature that can be noticed is that the model predicts the moonlit sky to be redder than

Figure 5: Example isophotal *alt-az* map for the expected moonlight contribution. The dashed white lines trace the loci at constant angular distance from the moon, while the two dotted red lines indicate the extreme apparent lunar paths during a full Saros cycle.

Filter: B   Moon Elevation: 20.0   FLI: 0.50
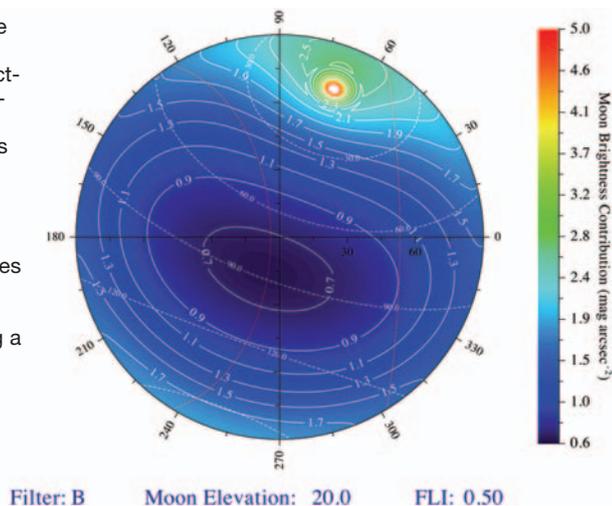
observed, since the *B* data points are systematically brighter than the model, while for *R* and *I* the opposite is true.

Due to the large number of input parameters involved in the KS model, the overall effects of moonlight are better understood with the use of isophotal maps, one example of which is presented in Fig. 5. The calculations were done in the *B* passband, using the broadband extinction coefficients measured on Paranal (Patat 2003), for FLI=0.5 (half moon) and moon elevation 20 degrees. The *alt-az* map shows the isophotal contours (solid white lines), the moon-target angular separation (dashed white lines) and the region spanned by the moon's apparent paths during the 18 years Saros cycle computed for Paranal (dotted red curves). As one can see the minimum surface brightness (0.6 mag arcsec^{-2}) is attained at about 80 degrees from the moon, on the great circle passing through zenith and the moon itself. Actually, computing several models for different moon positions and different passbands, it is easy to verify that while the minimum lies always on that great circle, its angular distance from the moon is 90 degrees when the moon is close to the horizon (see for example Fig. 1), while it tends to decrease for higher moon elevations, reaching about 60 degrees when the moon is at zenith. The opposite happens to the minimum surface brightness, which steadily grows with moon elevation, reaching its maximum when the moon culminates. Of course, the exact value of minimum surface brightness and the isophotal shape depends on the passband; in the case of the example reported in Fig. 5, the minimum surface brightness enhancement is 0.4 mag arcsec^{-2}, reached when the moon rises or sets, while this value grows to about 1.3 mag arcsec^{-2} when the moon is at zenith. Finally, to evaluate the effects produced by scattered light when the moon is below the horizon, we have included the moon twilight, following the prescriptions given by Schaefer (1998). According to the model, the *B* sky brightness enhancement is

smaller than 0.1 mag arcsec^{-2} on the whole sky when the full moon is more than five degrees below the horizon. This reduces to one degree when FLI=0.5.

The main conclusion is that there are regions of the sky where the moon contamination can be minimized, and this has important consequences in the optimisation of Service Mode observations of programmes that can be executed in grey or bright time.

Towards a New Perspective

As far as moon illumination is concerned, astronomical programmes are generally classified as suitable for dark or bright time. In the case of ESO, the programmes are actually grouped into three classes, according to the user required FLI: dark (FLI<0.4), grey (0.4<FLI<0.7) and bright (FLI>0.7). Taking into account that the time when FLI<0.4 and the moon is below the horizon is also considered as dark time, grey and bright fractions account for 11% and 32% of the total observing time respectively. Therefore, there is a substantial amount of time in which the moon contribution is significant and that, for the same reason, is normally used for IR observations, which are essentially not affected by the moon presence. In fact, the considerations we have been developing here are relevant to optical instruments only.

At present, ESO requests Service Mode users to specify the maximum acceptable FLI and the minimum acceptable angular distance to the moon at the time of defining their observation blocks. While these two parameters alone do not suffice to accurately predict the sky brightness at the target position as we have discussed, they do provide a simple set of constraints whose fulfilment can be predicted in advance and still allow the user to have a fair amount of control on the sky brightness conditions under which the observations will be executed. Furthermore, they do not severely constrain the short-term scheduling flexibility that is

essential to the efficiency of Service Mode observing. However, experience has shown that users often tend to request a moon-target separation larger than needed. This, besides reducing the observability window, does not necessarily guarantee that the sky background is minimized. In fact, as we have seen in the previous section, under certain circumstances a separation of 70 degrees is better than one of 120 degrees.

In the long run, it may be possible to directly incorporate the sky brightness at the target position as a constraint. This will require a well calibrated model for the scattered moonlight allowing the night time operations astronomers to estimate in an accurate and straightforward manner the expected sky brightness. To this end, it will be necessary to develop and test more sophisticated models and to obtain extensive datasets sampling the parameter space well. As far as the models are concerned, Krisciunas & Schaefer proposed a series of improvements on their own model in order to increase its predictive power, already in their original work. As a matter of fact, extensions and refinements of the KS model are currently in progress (K. Nordsieck, private communication). Regarding the experimental side, besides the *V* data published by Krisciunas & Schaefer and the first *BVRI* data set presented by Patat (2003), which were collected only as a by-product of the night sky survey, to our knowledge no other systematic observing campaigns have been carried out. Collecting a large database containing measurements of sky brightness obtained through multiple filters and sampling as wide a parameter space as possible is a considerable effort, which may perhaps be best undertaken by coordinating dedicated small-sized telescopes. Nevertheless, the outcome of such a project, resulting in an improved ability to predict the actual observing conditions, can be regarded as a necessary step in maximizing the efficiency of the precious observing time at current and future large telescopes.

References

Hayes, D.S. & Latham, D. W., 1975, ApJ, 197, 593
Krisciunas, K., 1990, PASP, 102, 1052
Krisciunas, K. & Schaefer, B. E., 1991, PASP 103, 1033
Kurucz, R.L., 1993, Kurucz CD-ROM No. 13
Patat, F., 2003, A&A, 400, 1183
Schaefer, B. E., 1998, Sky & Telescope, May 1998, p.57
v. d. Hulst, H.C., 1957, Light Scattering by Small Particles, John Wiley & Sons, New York
Walker, A., 1987, N.O.A.O. Newsletter, No. 10, 16